inorganics

MDPI

Article

On the Aqueous Solution Behavior of *C*-Substituted 3,1,2-Ruthenadicarbadodecaboranes

Marta Gozzi, Benedikt Schwarze, Peter Coburger and Evamarie Hey-Hawkins *

Institute of Inorganic Chemistry, Leipzig University, Johannisallee 29, 04103 Leipzig, Germany
* Correspondence: hey@uni-leipzig.de; Tel.: +49-341-9736151

Received: 26 June 2019; Accepted: 16 July 2019; Published: 22 July 2019

Abstract: 3,1,2-Ruthenadicarbadodecaborane complexes bearing the $[C_2B_9H_{11}]^{2-}$ (dicarbollide) ligand are robust scaffolds, with exceptional thermal and chemical stability. Our previous work has shown that these complexes possess promising anti-tumor activities in vitro, and tend to form aggregates (or self-assemblies) in aqueous solutions. Here, we report on the synthesis and characterization of four ruthenium(II) complexes of the type [3-(η^6-arene)-1,2-R_2-3,1,2-$RuC_2B_9H_9$], bearing either non-polar (R = Me (**2**–**4**)) or polar (R = CO_2Me (**7**)) substituents at the cluster carbon atoms. The behavior in aqueous solution of complexes **2**, **7** and the parent unsubstituted [3-(η^6-*p*-cymene)-3,1,2-$RuC_2B_9H_{11}$] (**8**) was investigated via UV-Vis spectroscopy, mass spectrometry and nanoparticle tracking analysis (NTA). All complexes showed spontaneous formation of self-assemblies (10^8–10^9 particles mL^{-1}), at low micromolar concentration, with high polydispersity. For perspective applications in medicine, there is thus a strong need for further characterization of the spontaneous self-assembly behavior in aqueous solutions for the class of neutral metallacarboranes, with the ultimate scope of finding the optimal conditions for exploiting this self-assembling behavior for improved biological performance.

Keywords: metallacarborane; ruthenium; aggregation; UV-Vis spectroscopy; NTA

1. Introduction

Metallacarborane complexes of the icosahedral type can be roughly divided into two categories: those which feature an *exo*-polyhedral bond to a metal ion, and those where the metal is coordinated by an approximately planar open face of the carborane cluster, e.g., the C_2B_3 open face of *nido*-$[C_2B_9H_{11}]^{2-}$, commonly known as "dicarbollide" (see Appendix A for cluster nomenclature) [1]. Complexes belonging to the latter typically show *closo* structures, formally derived from the parent $C_2B_{10}H_{12}$ clusters by replacement of a BH unit with an isolobal metal complex fragment (Figure 1), which therefore contributes three orbitals to the cluster bonding [2].

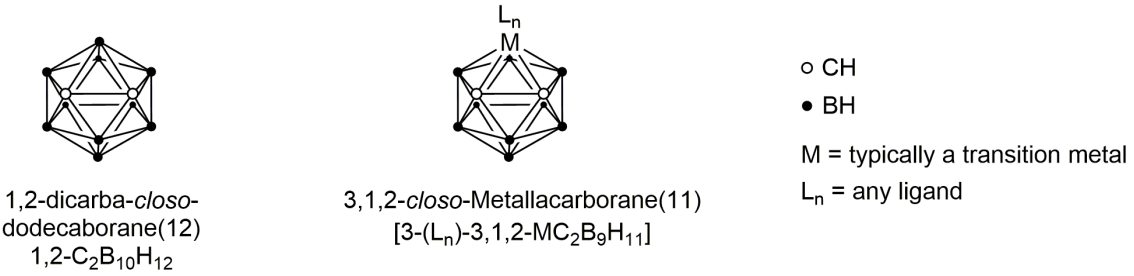

Figure 1. General structure of 1,2-dicarba-*closo*-dodecaborane(12) (**left**) and 3,1,2-*closo*-metallacarboranes(11) (**right**). Only one isomer per each structure is shown. For cluster nomenclature see Appendix A.

One main motivation that pushes investigations on the chemistry and physico-chemical properties of metallacarboranes is the long-known isolobal analogy between the cyclopentadienyl ($C_5H_5^-$, Cp^-) ligand and the dicarbollide $C_2B_9H_{11}^{2-}$ cluster [3]. This is, in turn, reflected in the types of application which have been investigated for metallacarborane complexes, ranging from catalysis [4], to medicine [5] and materials science [6] where often the performance of the metallacarborane is evaluated in comparison to analogous Cp-based complexes (see, for example, Grishin et al. in *Pol. Sci.* (2015) [7], and Louie et al. in *J. Med. Chem.* (2011) [8]).

Recently, we have focused on mixed-sandwich ruthenacarborane complexes of the type *closo*-[3-(η^6-arene)-3,1,2-$RuC_2B_9H_{11}$] (with arene = *p*-cymene, biphenyl, 1-Me-4-CO_2Et-C_6H_4), and on half-sandwich molybdacarboranes of the type [3-{L-κ^2*N*,*N*}-3-$(CO)_2$-*closo*-3,1,2-$MoC_2B_9H_{11}$] (with L = *N*,*N*-chelating ligand) for potential applications in medicine, specifically as anti-tumor agents [9,10]. In our previous investigations, we showed that the ruthenacarboranes are chemically exceptionally stable compounds under biologically relevant conditions and possess moderate anti-proliferative activities in vitro against human colorectal carcinoma and breast adenocarcinoma cell lines, and a 10× higher selectivity towards cancer cell lines than to healthy cells (primary fetal fibroblasts and macrophages). Moreover, spectrophotometric studies on aqueous solutions of *closo*-[3-(η^6-biphenyl)-3,1,2-$RuC_2B_9H_{11}$] strongly suggested a tendency to form aggregates, at low micromolar concentrations of the complex [9]. The dynamics of aggregation for the anionic metallacarboranes of type [*commo*-3,3′-$Co(1,2\text{-}C_2B_9H_{11})_2]^-$ (COSAN) are broadly studied in the literature [11–13], and these complexes are generally described as non-classical amphiphiles which spontaneously self-assemble into nano- or microstructures [14]. On the other hand, no studies are found on the aggregation properties of neutral *closo*-metallacarboranes. Moreover, for potential application in medicine, characterization of the aggregation behavior of a drug candidate is of primary importance, for ensuring validity and reproducibility of the biological tests, as already discussed for aggregate-based organic inhibitors [15]. Here, we report a small series of 3,1,2-ruthenadicarbadodecaborane(11) complexes, bearing either polar (R = CO_2Me) or non-polar (R = Me) groups at the carbon atoms of the dicarbollide ligand. The complexes were fully characterized, and the formation of aggregates in aqueous solutions was investigated via UV-Vis spectroscopy, mass spectrometry, and nanoparticle tracking analysis (NTA).

2. Results and Discussion

2.1. Synthesis and Characterization of Complexes **2**–**4** *and* **7**

Complex **2**, which bears a *p*-cymene ligand, is a known compound and was synthesized according to the literature [16]. Complexes **3** and **4** (Figure 2) were synthesized in moderate yields (45% for **3**, 32% for **4**), in an analogous way as previously reported [9], from Tl[3-Tl-1,2-Me_2-3,1,2-$C_2B_9H_9$] (**1**) and the respective ruthenium(II)–arene dimer [{(η^6-arene)RuCl(μ-Cl)}$_2$] (arene = biphenyl or 1-Me-4-CO_2Et-C_6H_4). The spectroscopic data for complexes **2** to **4** are in accordance with those reported for mixed-sandwich *closo*-ruthenacarboranes, which also incorporate an arene ligand [9,17–19].

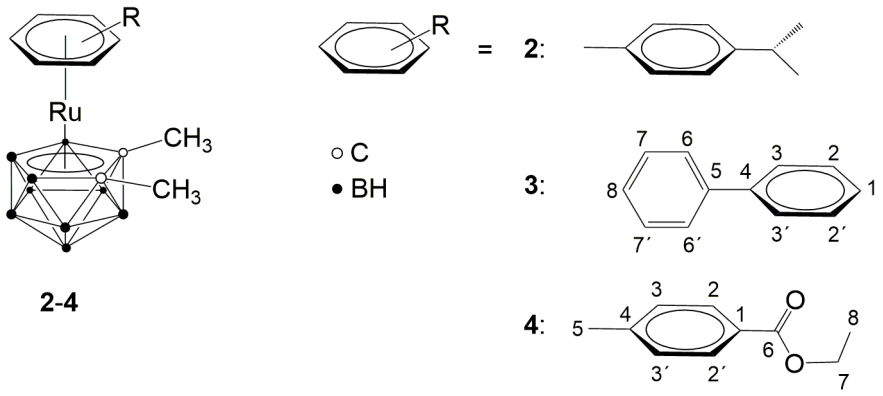

Figure 2. Structure of complexes **2** to **4**.

Complex **7** was synthesized in three steps from 1,2-$(CO_2Me)_2$-*closo*-1,2-$C_2B_{10}H_{10}$ (**5**) (Scheme 1). **5** was deboronated under mild conditions (MeCN/H_2O (2:1) (*v*/*v*) at room temperature) [20], to avoid cleavage of the $C_{cluster}$–CO_2Me *exo*-skeletal bonds. For the deprotonation of **6**, thallium(I) ethanolate was used as base at low temperature (−30 °C), instead of the KOH/thallium(I) acetate couple at 0 °C, used by Safronov et al. for the deprotonation of unsubstituted [*nido*-7,8-$C_2B_9H_{12}$]$^-$ [21], to avoid base-promoted cleavage of the methoxy ester.

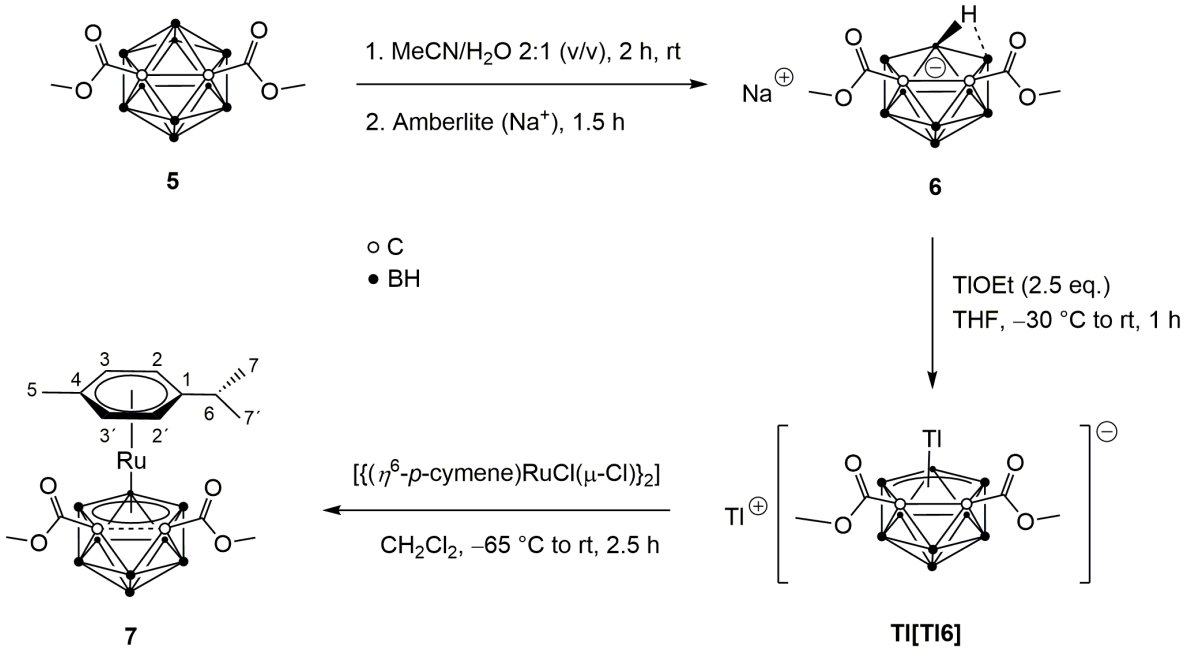

Scheme 1. Synthesis of **7** from 1,2-$(CO_2Me)_2$-*closo*-1,2-$C_2B_{10}H_{10}$ (**5**).

The weighted average (see definition in Appendix B) of the ^{11}B NMR signals of **7** is +3.5 ppm, which is in accordance to previously reported values for *pseudocloso*-ruthenacarborane structures [16,22] that are formally derived from a *closo* structure via breaking of the $C_{cluster}$–$C_{cluster}$ bond. In comparison, the weighted average of the ^{11}B signals for **2**, **3**, and **4** is −13.6, −12.8, and −11.7 ppm, respectively, which indicates *closo* structures. *X*-ray diffraction analysis of single crystals of **4** and **7** confirmed the *closo* and *pseudocloso* structures (Figure 3), with C(1)···C(2) distances of 1.680(5) Å and 2.243(2) Å, respectively. It is not unexpected that complex **7** presents a *pseudocloso* structure, since *closo*-to-*pseudocloso* cluster deformation is a commonly encountered phenomenon in ruthenacarborane complexes, when carbon-bound substituents introduce additional electron density into the $C_{cluster}$–$C_{cluster}$ bond, as in the case of phenyl substituents reported by Brain et al. and Bould et al. [16,22]. The structural

distortions in **7** are generally in accordance with those reported by Welch and co-workers for *pseudocloso*-[3-(η^6-arene)-1,2-Ph_2-3,1,2-$RuC_2B_9H_9$] [22]. For example, the Ru–B(6) distance in **7** is 2.979(2) Å, which is 0.5 Å shorter than in the corresponding undistorted *closo*-[3-(η^6-*p*-cymene)-3,1,2-$RuC_2B_9H_{11}$] (**8**) (Table 1) [9], and the B(6)–B(10) and the C(1)–B(4) bonds are 1.885(2) Å (vs. 1.759(1) Å in **8**) and 1.636(2) Å (vs. 1.718(1) Å in **8**), respectively. The B(4)–B(5) bond is, however, 0.04 Å longer in the *pseudocloso* structure **7**, compared to the *closo* one (**8**), in contrast to what was observed by Welch for diphenyl-substituted *pseudocloso*-[3-(η^6-arene)-1,2-Ph_2-3,1,2-$RuC_2B_9H_9$] complexes, with respect to the corresponding *closo*-1,2-Ph_2-$C_2B_{10}H_{10}$ [22].

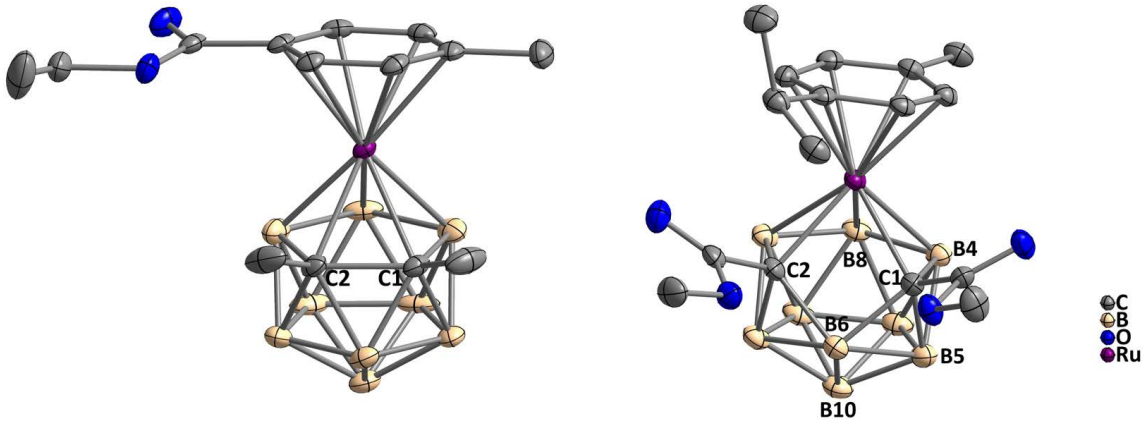

Figure 3. Molecular structures of **4** (**left**) and **7** (**right**). Thermal ellipsoids are shown at the 50% probability level. Hydrogen atoms are omitted for clarity. Numbering of selected boron and carbon positions is given.

Table 1. Selected bond lengths, distances (Å) and angles (°) in **4** and **7**, and the respective unsubstituted ruthenacarboranes **8** and **9**.

	[3-(η^6-*p*-cymene)-3,1,2-$RuC_2B_9H_{11}$] (**8**) [a]	**7**	[3-{η^6-(4-Me-1-COOEt-C_6H_4)}-3,1,2-$RuC_2B_9H_{11}$] (**9**) [a]	**4**
Ru–Ctd1 [b]	1.714(4)	1.768(1)	1.708(2)	1.738(1)
Ru–Ctd2 [b]	1.619(4)	1.485(1)	1.623(2)	1.598(1)
Ru–B(C_2B_3 face) [c]	2.203(3)	2.216(2)	2.205(8)	2.195(5)
Ru–C(C_2B_3 face) [c]	2.171(2)	2.127(2)	2.166(5)	2.171(3)
Ru–C(arene) [c]	2.224(3)	2.265(2)	2.217(7)	2.237(3)
C–C(cluster)	1.627(4)	2.243(2)	1.623(3)	1.680(5)
B–B [d]	1.774(7)	1.799(3)	1.778(7)	1.772(7)
B–C(cluster) [c]	1.720(5)	1.662(3)	1.719(3)	1.722(6)
C(cluster)–C(exo) [c]	–	1.497(1)	–	1.517(5)
Ru–B(6)	3.494(1)	2.979(2)	–	–
B(6)–B(10)	1.759(1)	1.885(2)	–	–
B(4)–B(5)	1.797(1)	1.838(3)	–	–
C(1)–B(4)	1.718(1)	1.636(2)	–	–
C(1)–B(5)	1.696(1)	1.614(2)		
Deviation from coplanarity [e]	5.11(9)	2.5(1)	2.3(5)	6.3(1)
Ru–C(1)–B(6)	126.79(3)	100.12(9)	–	–
C(1)–B(6)–C(2)	55.99(2)	88.7(1)	–	–
B(6)–C(2)–Ru	126.49(5)	100.14(9)	–	–
C(2)–Ru–C(1)	44.02(4)	69.75(6)	–	–

[a] From [9]. [b] Ctd1 = centroid of the C_6 ring of the arene ligand. Ctd2 = centroid of the C_2B_3 face of the dicarbollide ligand. [c] Average value. [d] Average B–B value. For **7**, the B(6)–B(10) bond length is not included. [e] Deviation from coplanarity of the arene and dicarbollide ligands was measured between the least-squares plane formed by the C_6H_4 ring of the arene ligand, and the least-squares plane formed by the lower boron belt (B_5H_5) of the cluster, as reported previously [9].

2.2. ^{11}B NMR Spectra of Complex 3

Complexes **2**–**4** and **7** show moderate to good solubility in chloroform and dichloromethane, and good solubility in dimethylsulfoxide (DMSO). No displacement of either the arene or the (substituted) dicarbollide ligands occurred in wet DMSO-d_6, at room temperature for over a month,

in all complexes, as evidenced by ^{1}H and ^{11}B NMR spectroscopic analysis (Figures S1 and S2 in Supplementary Materials). This is in analogy to what was previously observed for unsubstituted *closo*-[3-(η^6-arene)-3,1,2-$RuC_2B_9H_{11}$] complexes [9], supporting the use of ruthenacarboranes as stable organometallic scaffolds for applications in medicine.

The ^{11}B NMR spectra of complex **3** deserve special attention. In addition to the four (in DMSO-d_6) or five (in CD_2Cl_2) doublets for the nine boron atoms of the [η^5-(7,8-Me_2-*nido*-7,8-$C_2B_9H_9$)]$^{2-}$ ligand, additional low-intensity ^{11}B signals are present in the region 0 to −20 ppm (Figure 4), which are unlikely due to impurities from the sample, as confirmed by elemental analysis. These low-intensity signals are instead most likely due to solvent effects on the dicarbollide cluster, which are already described in the literature for decaborane in terms of solvent polarizability that can give rise to additional peaks or shoulders in the ^{11}B NMR spectra [23]. Particularly noteworthy is the small broad signal at +19.8 ppm (Figure 4, bottom), which is present in DMSO-d_6 solution, but not in CD_2Cl_2. The small peak is present already in freshly dissolved samples of **3** in wet DMSO-d_6 and remains stable in shift and intensity over one month.

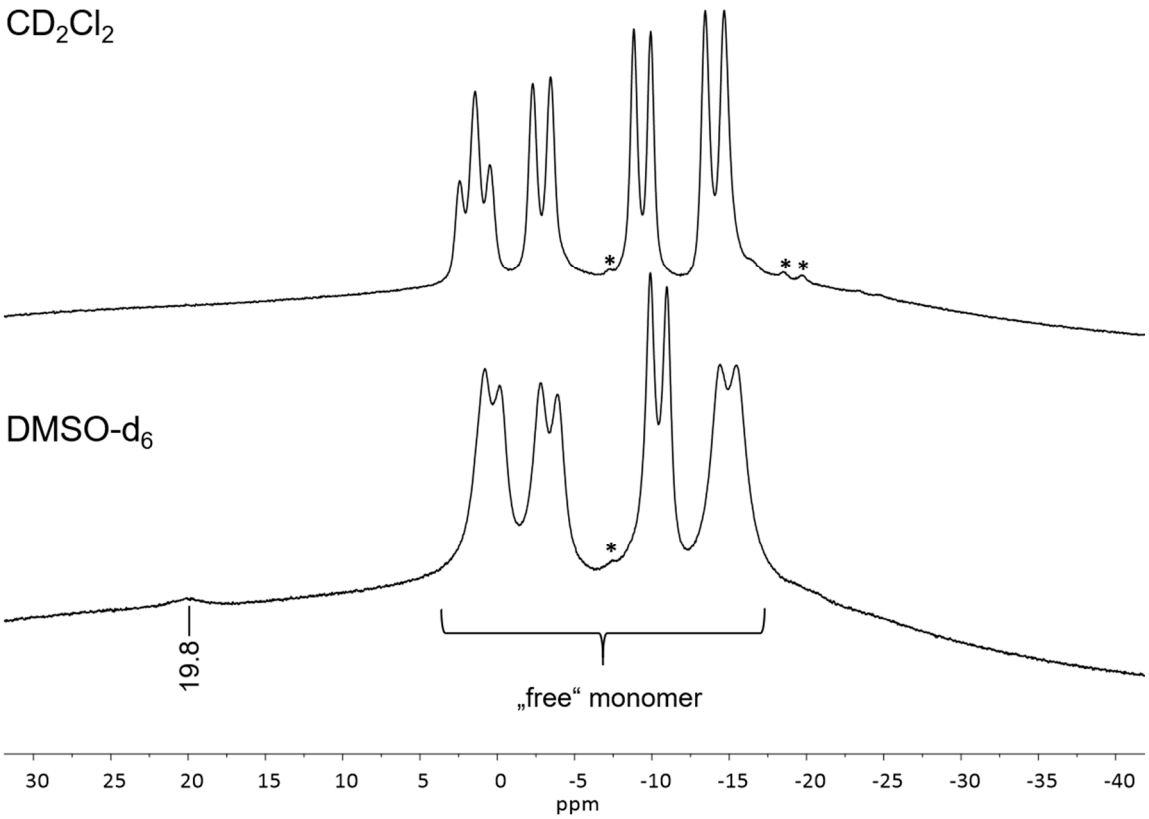

Figure 4. ^{11}B NMR spectra (at 128.83 MHz) of **3** freshly dissolved in CD_2Cl_2 (**top**) and wet DMSO-d_6 (**bottom**). Signals for monomeric **3** and the signal for self-assemblies of **3** are observed in DMSO-d_6, as suggested by Deore et al. and Crociani et al. [24,25]. * marks the low-intensity additional ^{11}B signals, probably due to solvent effects.

This cannot be attributed to the protonated uncoordinated *nido*-carborane(−1) ligand. Deore et al. and Crociani et al. showed that the chemical shift of the ^{11}B NMR signals is sensitive to changes in coordination geometry at the boron atom (trigonal at 20 to 30 ppm vs. tetrahedral at 5 to 10 ppm), and that such shifts could be used to distinguish between nano-sized polymeric structures and monomeric forms in solution [24,25]. The signal at +19.8 ppm in the ^{11}B NMR spectrum of **3** could, therefore, be due to the presence of self-assembled nano-structures of **3** in solution, which rapidly

interchange with monomers of **3**, which are, under the conditions of the NMR experiment, still the dominant species in solution.

The interpretation of the ^{11}B NMR data of potentially aggregating carborane-containing compounds is, however, not trivial and remains somewhat confusing and elusive in the literature. Just to give an example, Bonechi et al. investigated the solution behavior of sugar-substituted *closo-ortho*-carboranes via ^{1}H and ^{11}B NMR spectroscopy in parallel under aggregating (D_2O) and "non-aggregating" conditions (C_2D_5OD) [26]. In the $^{11}B\{^{1}H\}$ NMR spectra in both D_2O and C_2D_5OD, the presence of down-field shifted small peaks (ca. +20 ppm), analogous to that for complex **3** in DMSO-d_6, is evident, but no rational behind this was proposed. It was simply concluded by the authors that there is no difference in the NMR spectra between aggregating and "non-aggregating" conditions, although it is not clear why an ethanolic solution should represent "non-aggregating" conditions, since *closo*-carborane derivatives are also known to form nano-structures in ethanol [27].

2.3. UV-Vis Spectroscopy, Mass Spectrometry and Nanoparticle Tracking Analysis (NTA)

The behavior of **2**, **7** and the parent unsubstituted [3-(η^6-*p*-cymene)-3,1,2-$RuC_2B_9H_{11}$] (**8**) in aqueous solution was investigated, via UV-Vis spectroscopy, mass spectrometry and nanoparticle tracking analysis (NTA). The three ruthenacarborane complexes bear the same arene ligand (*p*-cymene) and differ only in the type of substituents at the cluster carbon atoms (methyl (**2**), CO_2Me (**7**), and H (**8**)). UV-Vis spectra of **3**, which bears a biphenyl ligand, were also measured, to support the ^{11}B NMR data.

UV-Vis spectroscopy is a useful technique for studying both absorption and scattering phenomena, since the UV-Vis spectrum (ε_λ) is the result of two components, namely absorption and scattering [28]. The two phenomena can be distinguished, and sometimes separated, based on their different dependency on the wavelength (λ), $\varepsilon \propto \lambda$ for absorption, and $\varepsilon \propto \lambda^{-4}$ for Rayleigh scattering, respectively. The UV-Vis spectra of **2**, **7**, and **8** in phosphate-buffered saline (PBS)/DMSO mixtures do not show a clear absorption maximum in the range of 250 to 550 nm, whereas complex **3** has an absorption maximum at 290 nm (Figure 5).

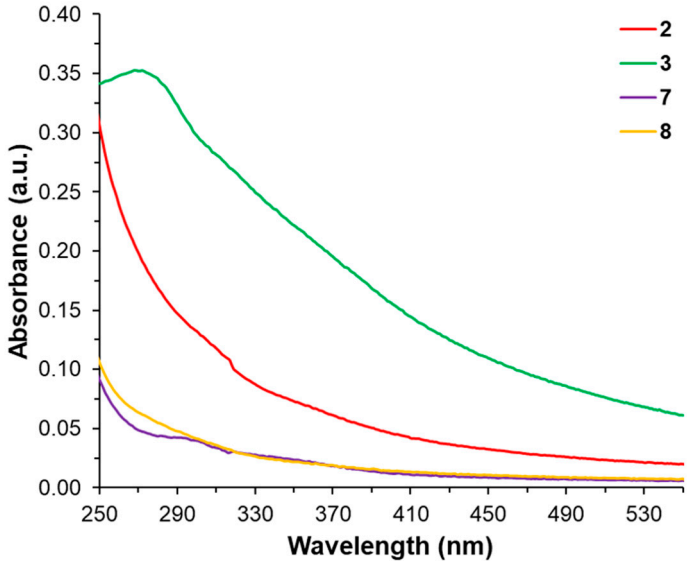

Figure 5. UV-Vis spectra of **2**, **3**, **7**, and **8** in PBS/DMSO mixtures. Content of DMSO is 1 vol % for all samples. [ruthenacarborane] = 20 μM. Spectra are corrected via subtraction of the blank (PBS + 1 vol % DMSO).

The absorbance shows, however, for all four complexes, an exponential increase towards the blue region of the spectrum, which approximates the case limit of pure Rayleigh scattering. Increasing the concentration of the ruthenacarboranes up to 50 μM only increased the intensity of the exponential

decay of the spectrum, and no absorption maxima were visible. Scattering is thus the major component of the absorbance spectra of **2**, **3**, **7**, and **8**, although the scattering intensity of **7** and **8** is much lower than for **2** and **3**. This suggests the presence of self-assemblies of the ruthenacarborane complexes in PBS/DMSO mixtures, albeit, possibly, in different concentrations. Complex **3** shows the highest scattering intensity of the series, i.e., the highest concentration of aggregates in solution, which is likely the reason why aggregation could also be observed in its ^{11}B NMR spectrum in DMSO-d_6 (see above), but not in the spectra of **2** and **7**, nor in the previously reported ^{11}B NMR spectra of **8** [9].

ESI mass spectra of **2**, **7**, and **8** in MeCN/H_2O (98:2, *v*/*v*) mixtures show a rather complicated fragmentation, with many, partially overlapping, isotopic patterns of carborane-containing species (Figure 6 (**2**) and Figure S3 (**7**,**8**) in Supplementary Materials). In the case of **2**, for example, both the monomer ([M + Na]$^+$), the dimer ([2M + Na]$^+$), and the trimer ([3M + NH_4]$^+$) were found in the ESI(+) mass spectrum, together with many other peaks, which could not be unequivocally assigned (see the peaks marked with * in Figure 6). Moreover, reproducibility of the MS fragmentation patterns was very poor for all three complexes under the same experimental conditions, which suggests a random and uncontrolled spontaneous self-assembly in solution. From the analysis of the mass spectra alone, one might thus infer that the compound is not pure. Fortunately, the other analytical techniques used to characterize compounds **2**, **7**, and **8**, i.e., NMR and IR spectroscopy, X-ray diffraction, and elemental analysis, clearly indicate that the complexes are analytically pure and void of any kind of impurities.

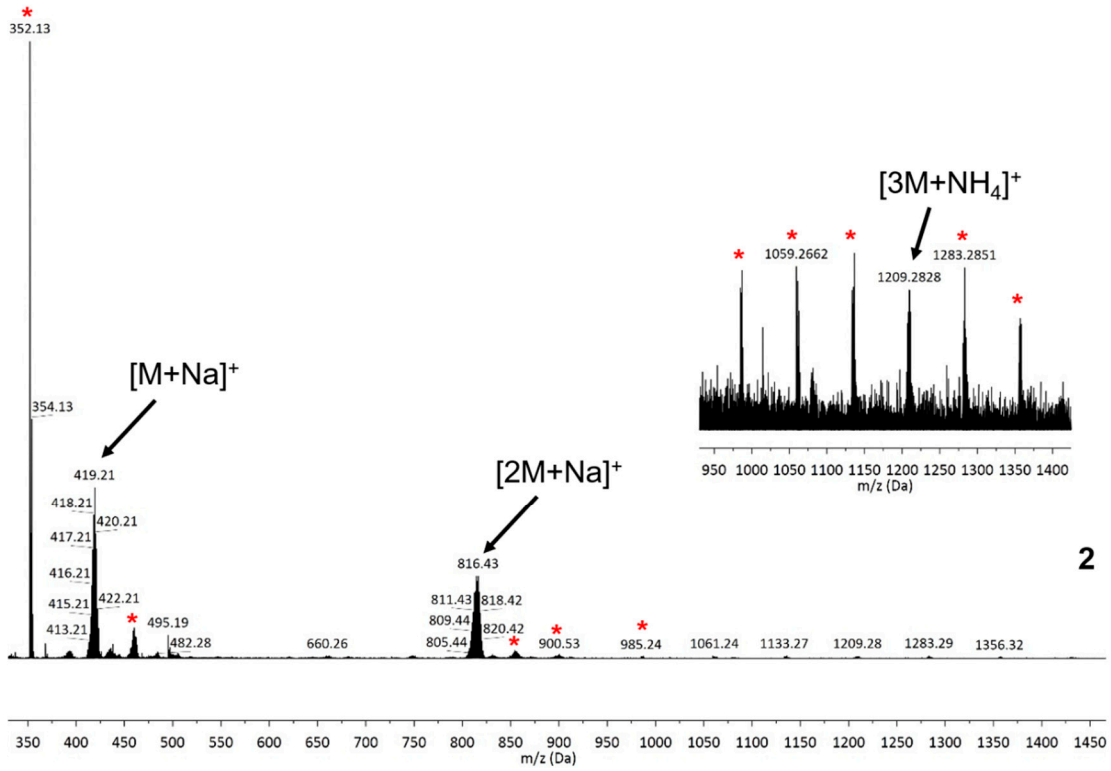

Figure 6. ESI(+) mass spectrum of **2** (M = 397.22), measured in MeCN/H_2O (98:2, *v*/*v*). The peaks which could not be unequivocally assigned are indicated by *. The inset shows a section of the region *m*/*z* = 950 to 1400.

Samples of **2**, **7**, and **8** in PBS/DMSO mixtures were also measured via nanoparticle tracking analysis (NTA) to estimate the relative concentration, size, and size distribution of self-assemblies in solution observed by ESI mass spectrometry and UV-Vis spectroscopy. Nanoparticle tracking analysis (NTA) is a fairly new technique for the measurement of colloidal and nano-sized suspensions, which was first commercialized in 2006 by NanoSight Ltd, Salisbury, UK [29]. It has been used for the study of different kinds of samples, ranging from atmospheric [30], to food [31] and to biological

samples [32]. The analysis principles and instrument set-up have been extensively discussed in the literature [33]. NTA is a light-scattering technique, in which particle tracking is based on the Brownian motion description of suspended particles in a fluid, captured simultaneously but individually by a charge-coupled device (CCD) camera. The software calculates size (hydrodynamic radius), size distribution, and concentration of the particles. NTA has the advantage over dynamic light scattering (DLS) methods in that it does not suffer from the known bias in size and size distribution of the latter. However, the applicability of NTA is limited to a narrow range of concentrations (10^6–10^9 particles mL^{-1}), and the calculated values of size and concentration are highly sensitive to capture and processing parameters, as discussed recently [34]. Samples of **2**, **7**, and **8** were therefore measured using the same capture and processing parameters, for direct comparison.

All three metallacarboranes form self-assemblies of nanometer size in PBS/DMSO mixtures at 25 °C, albeit in different concentrations, namely 10^8 for **7** and **8**, vs. 10^9 particles mL^{-1} for **2** (Figure 7 and Table S2 in Supplementary Materials). **2** shows a bimodal distribution of particle sizes, centered at 115 and 155 nm, respectively, but also presents a smaller fraction of particles with sizes up to 400 nm. Samples of **7** and **8** show broad size distributions of the particles, in the range of 95 to 300 nm (**7**) or 145 to 400 nm (**8**). Thus, all three complexes form fairly polydisperse self-assemblies in PBS/DMSO mixtures at room temperature, that is, under conditions, which approximate those of biological tests in vitro.

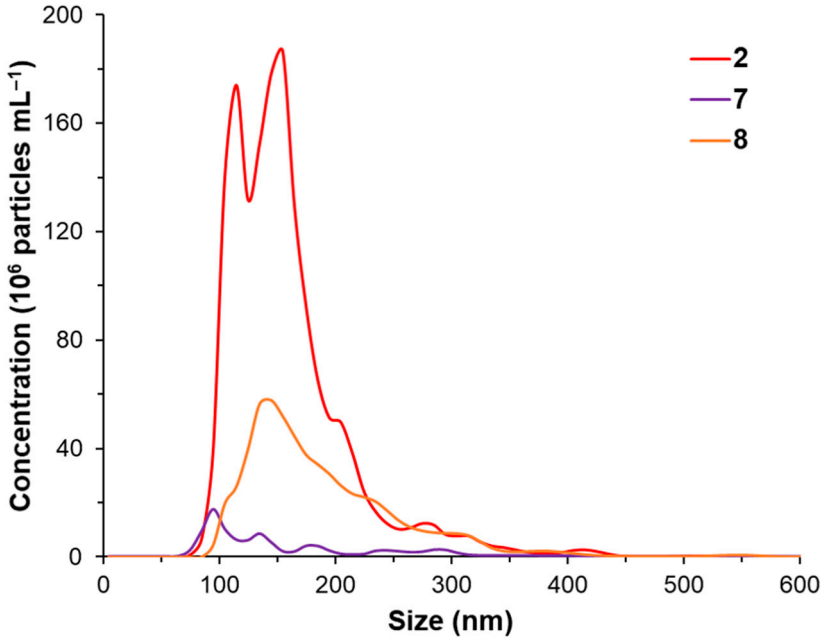

Figure 7. Size distribution of **2**, **7**, and **8** in PBS/DMSO mixtures, from nanoparticle tracking analysis (NTA). [**2**] = [**7**] = [**8**] = 20 μM. The dilution factor is the same for all samples. Content of DMSO was 1 vol % in all samples. Average data from five independent captures are shown. T = 25 °C. Particle concentrations and size values, with relative standard deviations, are given in Table S2 (Supplementary Materials).

As already mentioned before, aqueous self-assembly of neutral (metalla)carboranes has been so far poorly investigated, and is limited to a few examples of *C*-substituted *closo*-carboranes [26,27]. No studies on the effect of spontaneous aggregation on the biological activity profile or stability in the biological medium are found in the literature. Therefore, comprehensive multi-spectroscopic bioanalytical investigations are now underway.

3. Materials and Methods

3.1. General Procedures and Instrumentation

Chemicals were used as purchased. Phosphate-buffered saline (PBS) was purchased from Sigma Aldrich (Taufkirchen, Germany). Tl[3-Tl-1,2-Me_2-3,1,2-$C_2B_9H_9$] (**1**) [35–37], *closo*-[3-(η^6-*p*-cymene)-1,2-Me_2-3,1,2-$RuC_2B_9H_9$] (**2**) [16] and *closo*-[3-(η^6-*p*-cymene)-3,1,2-$RuC_2B_9H_{11}$] (**8**) [9] were synthesized as previously reported. Synthesis and characterization of **5** and **6** (precursor compounds) are given in the Supplementary Materials. All manipulations were carried out in a dry and oxygen-free nitrogen atmosphere using standard Schlenk techniques, unless otherwise stated. Thallium(I) ethanolate (Alfa Aesar©, Kandel, Germany) was stored under argon at −20 °C, protected from light. All manipulations involving thallium(I) compounds were performed wearing personal protective equipment as prescribed in the material safety data sheet (MSDS), and thallium(I)-containing waste was disposed of according to official regulations. Dried and degassed dichloromethane (CH_2Cl_2) and *n*-hexane were obtained from an MBRAUN solvent purification system (MB SPS-800, M. Braun Inertgas-Systeme GmbH, Garching, Germany) and stored under a nitrogen atmosphere over molecular sieves (4 Å). Tetrahydrofuran (THF) was dried over Na/benzophenone, freshly distilled prior to use and stored under nitrogen atmosphere over molecular sieves (4 Å). Acetonitrile (MeCN) was degassed, freshly distilled prior to use and stored under nitrogen. DMSO was dried over CaH_2, freshly distilled prior to use and stored under nitrogen over molecular sieves (4 Å).

Thin-layer chromatography (TLC) was carried out on precoated glass plates (Merck Silica Gel 60 F_{254}). Visualization of the compounds on TLC plates was achieved by means of an iodine chamber, or by treatment with a solution of $PdCl_2$ (1 wt % in MeOH). Column chromatography was carried out with silica gel (0.035–0.070 mm, 60 Å). NMR spectra were acquired at room temperature with a Bruker AVANCE III HD 400 MHz spectrometer (Bremen, Germany). ^{1}H (400.13 MHz) and ^{13}C{^{1}H} (100.16 MHz) NMR spectra were referenced to tetramethylsilane (TMS) as internal standard. ^{11}B (128.38 MHz) NMR spectra were referenced to the unified Ξ scale [38]. Mass spectrometry measurements were carried out with an ESI-MS Bruker ESQUIRE 3000 (Benchtop LC Iontrap, Bremen, Germany) spectrometer. FT-IR spectra were obtained with a PerkinElmer system 2000 FTIR spectrometer (Baesweiler, Germany), scanning between 400 and 4000 cm^{-1}. Elemental analyses were performed with a Heraeus VARIO EL oven (Lagenselbold, Germany). X-ray data were collected with a GEMINI CCD diffractometer (Rigaku Inc., Neu-Isenburg, Germany), using Mo-Kα radiation (λ = 0.71073 Å), T = 130(2) K and ω-scan rotation. Data collection and refinement data are given in Table S1 (Supplementary Materials). Absorption corrections were performed with SCALE3 ABSPACK [39]. The structures were solved by direct methods with SHELXS [40]. Structure refinement was done with SHELXL-2016 [41] by using full-matrix least-square routines against F^2. All non-hydrogen atoms were refined with anisotropic thermal parameters, and the HFIX command was used to locate all hydrogen atoms for non-disordered regions of the structure. Crystals of **4** and **7** contain no solvent molecules. The C_2 unit of the carborane cluster was located with bond length analysis. The pictures were generated with the program Diamond (version 3.2) [42]. CCDC 1915985 (**4**) and 1915986 (**7**) contain the supplementary crystallographic data for this paper. UV-Vis absorption spectra were measured with a PerkinElmer UV/VIS/NIR Lambda 900 spectrometer (Baesweiler, Germany), equipped with a xenon arc lamp, using quartz cuvettes (V = 3 cm^3). Spectra were recorded at 25 °C, in the range of 250 to 550 nm at 1.0 nm resolution. All measurements were corrected by subtracting the blank (PBS + 1 vol % DMSO). Nanoparticle tracking analysis (NTA) measurements were performed using the NanoSight LM10 instrument from Malvern Instruments Ltd. (Worcestershire, UK), containing a sample chamber of about 0.25 mL, and equipped with a 532 nm laser, a microscope LM14B, and a camera sCMOS. All measurements were performed at 25 ± 0.1 °C. Each sample was measured in five independent captures. The time of each capture was set to 60 s. The NTA 3.0 analytical software (NanoSight Ltd., Salisbury, UK) was used for both capture and processing.

3.2. Syntheses

3.2.1. *closo*-[3-(η^6-Biphenyl)-1,2-Me_2-3,1,2-$RuC_2B_9H_9$] (**3**)

Following Bould et al. [16], [{(η^6-biphenyl)RuCl(μ-Cl)}$_2$] (0.20 g, 0.31 mmol, 1.0 eq.) was dissolved in dry THF (15 mL) and cooled to 0 °C. **1** (0.52 g, 0.92 mmol, 3.0 eq.) was added in one portion, and the mixture was stirred at room temperature for 17 h. Silica (0.5 g) was then added to the brown-orange mixture and the solvent was evaporated in vacuo. The residue was purified via filtration through a short pad of silica gel (length = 5 cm, diameter = 2.5 cm) using CH_2Cl_2 as eluent, which yielded a single yellow band (R_f = 0.88 in CH_2Cl_2). The latter was collected and evaporated to dryness, yielding pure **3** as pale yellow, air-stable solid. **3** is soluble in CH_2Cl_2 and DMSO, and moderately soluble in $CHCl_3$. Yield: 35.0 mg (45%). ^{1}H NMR (CD_2Cl_2): δ (ppm) = 0.55–3.88 (br, B–*H*), 2.05 (6H, s, C_{cage}–C*H*$_3$), 6.08–6.21 (3H, m, H^1, H^2 and $H^{2'}$), 6.46 (2H, d, $^3J_{HH}$ = 5.7 Hz, H^3 and $H^{3'}$), 7.51 (3H, m, H^7, $H^{7'}$, and H^8), 7.74 (2H, dd, $^3J_{HH}$ = 8.3, 1.6 Hz, H^6 and $H^{6'}$). ^{11}B NMR (CD_2Cl_2): δ (ppm) = 2.4 (1B, d, $^1J_{BH}$ = 129 Hz), 0.5 (1B, d, $^1J_{BH}$ = 126 Hz), −2.9 (2B, d, $^1J_{BH}$ = 147 Hz), −9.4 (2B, d, $^1J_{BH}$ = 140 Hz), -14.1 (3B, d, $^1J_{BH}$ = 158 Hz). ^{13}C{^{1}H} NMR (CD_2Cl_2): δ (ppm) = 32.2 (s, C_{cage}–CH_3), 75.9 (s, C_{cage}), 88.9 (s, C^3 and $C^{3'}$), 90.7 (s, C^1), 91.1 (s, C^2 and $C^{2'}$), 106.0 (s, C^4), 128.1 (s, C^6 and $C^{6'}$), 129.2 (s, C^7 and $C^{7'}$), 129.8 (s, C^8), 133.5 (s, C^5). IR (KBr; selected vibrations): $\widetilde{\nu}$ (cm^{-1}) = 3079 (m, ν_{CHarom}), 2929 (m, ν_{CHcage}), 2561 (s, ν_{BH}), 2515 (s, ν_{BH}), 1455 (s, $\nu_{C=C}$), 1405 (m, $\nu_{C=C}$), 1387 (m), 1015 (s, ν_{CC}), 835 (m) 764 (s, ν_{BB}), 694 (s, ν_{BB}). ESI-MS(−): *m*/*z* = 865.2356 (100%, [2M + Cl]$^-$). Anal. calcd for $C_{16}H_{25}B_9Ru$ (415.74): C, 46.23; H, 6.06. Found C, 46.70; H, 6.20.

3.2.2. *closo*-[3-(η^6-(1-Me-4-COOEt-C_6H_4))-1,2-Me_2-3,1,2-$RuC_2B_9H_9$] (**4**)

4 was synthesized in an analogous manner as described for **3**, from [{(η^6-(1-Me-4-COOEt-C_6H_4))RuCl(μ-Cl)}$_2$] (0.20 g, 0.30 mmol, 1.0 eq.) and 1 (0.51 g, 0.90 mmol, 3.0 eq.). The crude product was recrystallized from CH_2Cl_2/acetone (10:1, *v*/*v*) at room temperature to yield yellow plates of pure **4**, suitable for single crystal *X*-ray diffraction analysis. **4** is an air-stable pale yellow solid, soluble in CH_2Cl_2, $CHCl_3$, and DMSO. Yield: 25.3 mg (32%). ^{1}H NMR (CD_2Cl_2): δ (ppm) = 0.56–3.96 (br, B–*H*), 1.39 (3H, t, $^3J_{HH}$ = 7.1 Hz, H^8), 2.12 (6H, s, $C_{cluster}$–C*H*$_3$), 2.42 (3H, s, H^5), 4.41 (2H, q, $^3J_{HH}$ = 7.1 Hz, H^7), 6.02 (2H, d, $^3J_{HH}$ = 6.4 Hz, H^3 and $H^{3'}$), 6.55 (2H, d, $^3J_{HH}$ = 6.4 Hz, H^2 and $H^{2'}$). ^{11}B NMR (CD_2Cl_2): δ (ppm) = 2.7 (1B, br s), 1.6 (1B, br s) (the two doublets centered at 2.7 and 1.6 ppm in the ^{11}B NMR spectrum are very broad, and it is therefore not possible to give accurate values of $^1J_{BH}$ coupling constants), −2.3 (2B, d, $^1J_{BH}$ = 147 Hz), −8.9 (2B, d, $^1J_{BH}$ = 140 Hz), −13.5 (3B, d, $^1J_{BH}$ = 160 Hz). ^{13}C{^{1}H} NMR (CD_2Cl_2): δ (ppm) = 14.0 (s, C^8), 19.0 (s, C^5), 31.7 (s, $C_{cluster}$–CH_3), 62.7 (s, C^7), 76.2 (s, $C_{cluster}$), 91.0 (s, C^2 and $C^{2'}$), 91.9 (s, C^3 and $C^{3'}$), 93.1 (s, C^1), 105.0 (s, C^4), 164.9 (s, C^6). IR (KBr; selected vibrations): $\widetilde{\nu}$ (cm^{-1}) = 3067 (w, ν_{CHarom}), 2982 (w, $\nu_{CHcluster}$), 2931 (w, $\nu_{CHcluster}$), 2563 (s, ν_{BH}), 2520 (s, ν_{BH}), 1720 (s, $\nu_{C=O}$), 1379 (s, ν_{CO}), 1369 (m, ν_{CO}), 1294 (s, ν_{CO}), 1015 (s, ν_{CC}), 881 (m), 776 (m, ν_{BB}). ESI-MS (−): *m*/*z* = 483.1953 (100%, [M + CO_2Me]$^-$). Anal. calcd for $C_{14}H_{27}B_9O_2Ru$ (425.73): C, 39.50; H, 6.39. Found C, 39.67; H, 6.50.

3.2.3. *pseudocloso*-[3-(η^6-*p*-Cymene)-1,2-(CO_2Me)$_2$-3,1,2-$RuC_2B_9H_9$] (**7**)

Deprotonation of the nido-carborane(*−1*) *precursor*. **6** (0.106 g, 0.39 mmol, 1.0 eq.) was dissolved in dry THF (6 mL) and cooled to −30 °C, protected from light. Thallium(I) ethanolate (0.243 g, 0.07 mL, 0.97 mmol, 2.5 eq.) was then added in one portion, causing immediate formation of a yellow precipitate. The mixture was allowed to warm to room temperature over one hour. Stirring was stopped and the mixture was left standing overnight. The supernatant solution was carefully removed via filtration, and the precipitate was washed with *n*-hexane (6 mL), THF (8 mL), and ethanol (3 mL). The yellow residue (**Tl[Tl6]**) was further dried in vacuo (10^{-3} mbar) (the thallium salt **Tl[Tl6]** was dried in vacuo without heating, because heating of a carborane dithallium salt promotes reprotonation to the *nido*-carborane(−1) species, as reported [43]) and used directly, without further purification.

Complexation reaction. [{(η^6-*p*-cymene)RuCl(μ-Cl)}$_2$] (86 mg, 0.14 mmol, 1.0 eq.) and **Tl[Tl6]** were placed in a Schlenk flask, thoroughly mixed and cooled to −65 °C. Degassed CH_2Cl_2 (10 mL) was then added, and the reaction mixture was left stirring for 1.5 h at −65 °C, then slowly warmed to room temperature, over one hour. The dark red-brown mixture was filtered, and the solution concentrated in vacuo to a 2 mL volume. Degassed silica was then added, and all volatiles were removed in vacuo. The residue was then purified via filtration through a silica gel pad (length = 10 cm, diameter 2.5 cm), under nitrogen atmosphere, using CH_2Cl_2 as eluent, which yielded a single orange band. The latter was collected and evaporated to dryness. The crude product was recrystallized from CH_2Cl_2/*n*-hexane (1.5:1, *v*/*v*) at −20 °C, to yield orange prisms of pure **7**, suitable for single crystal *X*-ray diffraction analysis. **7** is air-stable, soluble in $CHCl_3$, CH_2Cl_2, acetone, and DMSO. Yield: 54.0 mg (39%). ^{1}H NMR ($CDCl_3$): δ (ppm) = 0.53–3.38 (br, B–*H*), 1.33 (3H, d, $^3J_{HH}$ = 6.9 Hz, H^7 and $H^{7'}$), 2.32 (3H, s, H^5), 2.89 (1H, hept, $^3J_{HH}$ = 6.9 Hz, H^6), 3.78 (6H, s, OCH_3), 5.83 (2H, d, $^3J_{HH}$ = 6.3 Hz, $H^{2/2'}$ or $H^{3/3'}$), 5.88 (2H, d, $^3J_{HH}$ = 6.3 Hz, $H^{2/2'}$ or $H^{3/3'}$). ^{11}B NMR ($CDCl_3$): δ (ppm) = 27.7 (1B, d, $^1J_{BH}$ = 122 Hz), 11.1 (1B, d, $^1J_{BH}$ = 149 Hz), 8.7 (1B, d, $^1J_{BH}$ = 115 Hz), 0.11 (2B, d) (the $^1J_{BH}$ coupling constant could not be determined, due to overlap with the peak at -1.6 ppm), −1.6 (3B, d, $^1J_{BH}$ = 142 Hz), -21.8 (1B, d, $^1J_{BH}$ = 172 Hz). IR (KBr; selected vibrations): $\widetilde{\nu}$ (cm^{-1}) = 3076 (w, ν_{CHarom}), 2950 (w, $\nu_{CHcluster}$), 2548 (s, ν_{BH}), 1716 (s, $\nu_{C=O}$), 1482 (w, $\nu_{C=C}$), 1458 (w, $\nu_{C=C}$), 1431 (m, $\nu_{C=C}$), 1261 (s, ν_{CO}), 1110 (m, ν_{CC}), 1020 (m, ν_{CC}), 860 (w), 765 (w, ν_{BB}). ESI-MS(+): *m*/*z* = 483.1948 (100%, [M + H]$^+$), 519.1705 (6%, [M + K]$^+$). Anal. calcd for $C_{16}H_{29}B_9O_4Ru$ (483.76): C, 39.73; H, 6.04. Found C, 39.78; H, 5.92.

3.3. Preparation of **2**, **7**, *and* **8** *for UV-Vis Spectroscopy, Mass Spectrometry, and NTA Measurements*

Stock solutions of **2**, **3**, **7**, and **8** in DMSO (1.0 mM) were freshly prepared before measurements. An aliquot of the DMSO stock solution of **2**, **3**, **7** or **8** was added to a PBS solution (3 mL) so that the final concentration of metallacarborane was 20 μM. DMSO content was 1 vol % in all samples. The samples were measured via UV-Vis spectroscopy and nano tracking analysis (NTA) 30 min to one hour after preparation. Samples of **3** were only measured by UV-Vis spectroscopy. Capture and processing parameters for the NTA measurements were the same for all samples for direct comparison. Samples were measured undiluted.

Compounds **2**, **7**, and **8** (ca. 1.0 mg) were dissolved in a minimum amount of MeCN (a few μL) and brought to a final volume of 500 μL with MeCN/H_2O (98:2, *v*/*v*). The final concentration of ruthenacarborane was ca. 100 μM. Samples were measured via ESI mass spectrometry (positive and negative mode) within 5 h from preparation.

4. Conclusions

A small series of neutral 3,1,2-ruthenadicarbaborane(11) complexes bearing either non-polar (methyl, **2**–**4**) or polar (CO_2Me, **7**) groups at the cluster carbon atoms were synthesized and fully characterized. The complexes possess a *closo* (**2**–**4**) or *pseudocloso* (**7**) structure in analogy to other *C*-substituted ruthenacarboranes in the literature. ^{11}B NMR spectra of **3** in DMSO-d_6 suggested the presence of aggregates of the complex in solution, confirmed by spectrophotometric analysis of **3** in PBS/DMSO mixtures at 20 μM. Moreover, spontaneous self-assembly in aqueous solutions was observed for all tested complexes in PBS/DMSO and MeCN/H_2O mixtures, regardless of the specific type of substitution at the $C_{cluster}$ vertices. They form particles with diameters on the nanometer scale, with high polydispersity and concentrations ranging from 10^8 (**7** and **8**) to 10^9 (**2**) particles mL^{-1}.

This study thus suggests that for perspective applications in medicine there is a strong need for further characterization of the spontaneous self-assembly in aqueous solutions of this class of ruthenacarboranes, as well as other neutral metallacarboranes, with the ultimate scope of finding the optimal conditions for modulating the aqueous behavior of the complexes. These studies are currently underway.

Supplementary Materials: The following are available online at http://www.mdpi.com/2304-6740/7/7/91/s1, Synthesis and characterization of compounds **5** and **6**; Table S1: Crystal data for **4** and **7**; Figure S1: ^{1}H NMR spectra (400.13 MHz) of complexes **2**–**4** in wet DMSO-d_6 in air at room temperature, after one month; Figure S2: ^{11}B NMR spectra (128.83 MHz) of complexes **2**–**4** and **7** in wet DMSO-d_6 in air at room temperature, after one month; Figure S3: ESI(+) mass spectra of **7** (top) and **8** (bottom) measured in MeCN/H_2O (98:2, *v*/*v*); Table S2: Mean size and concentration of particles for PBS/DMSO solutions of **2**, **7** and **8**.

Author Contributions: M.G. designed the studies, performed the syntheses, analyzed data and wrote the paper; M.G. and B.S. performed the UV-Vis and the NTA experiments and analyzed the data; P.C. performed the single-crystal XRD measurements and solved the structures; E.H.-H. designed the studies and wrote the paper.

Funding: This work was supported by the Saxon State Ministry for Sciences and Arts (SMWK, doctoral grant for M.G.) [grant No. LAU-R-N-11-2-0615], the German chemical industry association (VCI, doctoral grant for B.S.) [grant No. 197021], the Studienstiftung des deutschen Volkes (doctoral grant for P.C.) and the Graduate School "Leipzig School of Natural Sciences—Building with Molecules and Nano-objects" (BuildMoNa).

Acknowledgments: We thank C. Zilberfain and I. Estrela-Lopis (Institute of Medicinal Physics and Biophysics, Leipzig University) for access to the NTA equipment and fruitful discussions on the NTA data and D. Maksimović-Ivanić and S. Mihatović (Institute for Biological Research "Siniša Stanković", University of Belgrade) for fruitful discussion on aggregating compounds for application in medicine.

Conflicts of Interest: The authors declare no conflict of interest.

Appendix A

Nomenclature adopted for carborane clusters (according to IUPAC convention): *closo* = 12-vertex icosahedral cluster, with (n − 1) skeletal electron pairs (n = total number of vertices); *nido* = 11-vertex open-face cluster, with (n − 2) skeletal electron pairs (n = total number of vertices); *ortho-*, *meta-*, *para-* = 1,2-, 1,7-, 1,12-dicarba-*closo*-dodecaborane(12), respectively. For numbering of the carborane clusters refer to the IUPAC project 2012-045-1-800 by Beckett et al., *Nomenclature for boranes and related species*, *Chemistry International* **2018**, *40*, 33.

Appendix B

The weighted average was calculated multiplying the chemical shift value of each ^{11}B signal by its relative intensity, and then dividing by the total number of ^{11}B signals of the spectrum.

References

1. Grimes, R.N. Metallacarboranes of the Transition and Lanthanide Elements. In *Carboranes*; Academic Press: Cambridge, MA, USA, 2016; pp. 711–903.
2. Grimes, R.N. Structure and Bonding. In *Carboranes*; Academic Press: Cambridge, MA, USA, 2016; pp. 7–18.
3. Brown, D.A.; Fanning, M.O.; Fitzpatrick, N.J. Molecular Orbital Theory of Organometallic compounds. 15. A Comparative Study of Ferrocene and π-Cyclopentadienyl-(3)-1,2-Dicarbollyliron. *Inorg. Chem.* **1978**, *17*, 1620–1623. [CrossRef]
4. Gozzi, M.; Schwarze, B.; Hey-Hawkins, E. Half- and Mixed-Sandwich Metallacarboranes in Catalysis. In *Handbook of Boron Science with Applications in Organometallics, Catalysis, Material Science and Medicine*; Hosmane, N.S., Eagling, R., Eds.; World Scientific, Ltd.: London, UK, 2018; pp. 27–80. ISBN 978-1786344410.
5. Gozzi, M.; Schwarze, B.; Hey-Hawkins, E. Half- and Mixed-Sandwich Metallacarboranes for Potential Applications in Medicine. *Pure Appl. Chem.* **2019**, *91*, 563–573. [CrossRef]
6. Núñez, R.; Tarrés, M.; Ferrer-Ugalde, A.; de Biani, F.F.; Teixidor, F. Electrochemistry and Photoluminescence of Icosahedral Carboranes, Boranes, Metallacarboranes, and Their Derivatives. *Chem. Rev.* **2016**, *116*, 14307–14378. [CrossRef]
7. Grishin, I.D.; Kiseleva, N.E.; Markin, A.V.; Chizhevsky, I.T.; Grishin, D.F. Synthesis of Functional Polymers Based on Methacrylic Monomers Using Ruthenium Carborane Complexes. *Polym. Sci. Ser. B* **2015**, *57*, 1–8. [CrossRef]
8. Louie, A.S.; Vasdev, N.; Valliant, J.F. Preparation, Characterization, and Screening of a High Affinity Organometallic Probe for α-Adrenergic Receptors. *J. Med. Chem.* **2011**, *54*, 3360–3367. [CrossRef]

9. Gozzi, M.; Schwarze, B.; Sárosi, M.-B.; Lönnecke, P.; Drača, D.; Maksimović-Ivanić, D.; Mijatović, S.; Hey-Hawkins, E. Antiproliferative Activity of (η^6-Arene)ruthenacarborane Sandwich Complexes Against HCT116 and MCF-7 Cell Lines. *Dalton Trans.* **2017**, *46*, 12067–12080. [CrossRef]
10. Schwarze, B.; Sobottka, S.; Schiewe, R.; Sarkar, B.; Hey-Hawkins, E. Spectroscopic and Electronic Properties of Molybdacarborane Complexes with Non-innocently acting Ligands. *Chem. Eur. J.* **2019**, *25*, 8550–8559. [CrossRef]
11. Tarrés, M.; Viñas, C.; González-Cardoso, P.; Hänninen, M.M.; Sillanpää, R.; Dord'ovič, V.; Uchman, M.; Teixidor, F.; Matějíček, P. Aqueous Self-Assembly and Cation Selectivity of Cobaltabisdicarbollide Dianionic Dumbbells. *Eur. J. Chem.* **2014**, *20*, 6786–6794. [CrossRef]
12. Uchman, M.; Ďord'ovič, V.; Tošner, Z.; Matějíček, P. Classical Amphiphilic Behavior of Nonclassical Amphiphiles: A Comparison of Metallacarborane Self-Assembly with SDS Micellization. *Angew. Chem. Int. Ed. Engl.* **2015**, *54*, 14113–14117. [CrossRef]
13. Zaulet, A.; Teixidor, F.; Bauduin, P.; Diat, O.; Hirva, P.; Ofori, A.; Viñas, C. Deciphering the Role of the Cation in Anionic Cobaltabisdicarbollide Clusters. *J. Organomet. Chem.* **2018**, *865*, 214–225. [CrossRef]
14. Fernandez-Alvarez, R.; Ďord'ovič, V.; Uchman, M.; Matějíček, P. Amphiphiles without Head-and-Tail Design: Nanostructures Based on the Self-Assembly of Anionic Boron Cluster Compounds. *Langmuir* **2018**, *34*, 3541–3554. [CrossRef]
15. Coan, K.E.D.; Shoichet, B.K. Stoichiometry and Physical Chemistry of Promiscuous Aggregate-Based Inhibitors. *J. Am. Chem. Soc.* **2008**, *130*, 9606–9612. [CrossRef]
16. Bould, J.; Kennedy, J.D. An Assessment of the Intercarbon Stretching Phenomenon in C-substituted "pseudocloso" {3,1,2-RuC_2B_9} Metalladicarbaboranes. *J. Organomet. Chem.* **2014**, *749*, 163–173. [CrossRef]
17. Garcia, M.P.; Green, M.; Stone, F.G.A.; Somerville, R.G.; Welch, A.J.; Briant, C.E.; Cox, D.N.; Mingos, D.M.P. Metallaborane Chemistry. Part 14. Icosahedral η^6-Arene Carbametallaboranes of Iron and Ruthenium: Molecular Structures of *closo*-[1-(η^6-C_6H_5Me)-2,4-Me-1,2,4-$FeC_2B_9H_9$] and *closo*-[3-(η^6-C_6H_6)-3,1,2-$RuC_2B_9H_{11}$]. *Dalton Trans.* **1985**, *11*, 2343–2348. [CrossRef]
18. Hanusa, T.P.; Huffman, J.C.; Todd, L.J. Synthesis of π-(Arene)metallocarboranes Containing Iron and Ruthenium. Crystal Structure of 3,1,2-(η^6-1,3,5-$(CH_3)_3C_6H_3$)$FeC_2B_9H_{11}$. *Polyhedron* **1982**, *1*, 77–82. [CrossRef]
19. Shaw, K.F.; Reid, B.D.; Welch, A.J. Synthesis and Characterisation of Metal Complexes of Ether Carbaboranes. Molecular Structures of d^6 ML_3, d^8 ML_2 and d^{10} ML Complexes of Mono- and Di-ether C_2B_9 Carbaborane Ligands, Showing the Progressive Importance of Secondary M···O Bonding. *J. Organomet. Chem.* **1994**, *482*, 207–220. [CrossRef]
20. Genady, A.R.; Tan, J.; El-Zaria, M.; Zlitni, A.; Janzen, N.; Valliant, J.F. Synthesis, Characterization and Radiolabeling of Carborane-Functionalized Tetrazines for Use in Inverse Electron Demand Diels–Alder Ligation Reactions. *J. Organomet. Chem.* **2015**, *791*, 204–213. [CrossRef]
21. Safronov, A.V.; Hawthorne, M.F. Novel Synthesis of 3-Iodo-*ortho*-Carborane. *Inorg. Chim. Acta* **2011**, *375*, 308–310. [CrossRef]
22. Brain, P.T.; Bühl, M.; Cowie, J.; Lewis, Z.G.; Welch, A.J. Synthesis and Characterisation of pseudocloso Iridium and Ruthenium Diphenyl Carbaboranes. Molecular Structures of 1,2-Ph_2-3-(η^6-C_6H_6)-3,1,2-*pseudocloso*-$RuC_2B_9H_9$ and 1,2-Ph_2-3-(cym)-3,1,2-*pseudocloso*-$RuC_2B_9H_9$ (cym = *p*-cymene) and Individual Gauge for Localised Orbitals Calculations on Carbametallaboranes. *Dalton Trans.* **1996**, *2*, 231–237.
23. Gaines, D.F.; Nelson, C.K.; Kunz, J.C.; Morris, J.H.; Reed, D. Solvent Effects on the Boron-11 and Proton NMR Spectra of Decaborane(14), $B_{10}H_{14}$. *Inorg. Chem.* **1984**, *23*, 3252–3254. [CrossRef]
24. Crociani, B.; Antonaroli, S.; Marini, A.; Matteoli, U.; Scrivanti, A. Mechanistic Study on the Coupling Reaction of Aryl Bromides with Arylboronic Acids Catalyzed by (Iminophosphine) palladium(0) Complexes. Detection of a Palladium(II) Intermediate with a Coordinated Boron Anion. *Dalton Trans.* **2006**, *22*, 2698–2705. [CrossRef]
25. Deore, B.A.; Yu, I.; Woodmass, J.; Freund, M.S. Conducting Poly(anilineboronic acid) Nanostructures: Controlled Synthesis and Characterization. *Macromol. Chem. Phys.* **2008**, *209*, 1094–1105. [CrossRef]
26. Bonechi, C.; Ristori, S.; Martini, S.; Panza, L.; Martini, G.; Rossi, C.; Donati, A. Solution Behavior of a Sugar-Based Carborane for Boron Neutron Capture Therapy: A Nuclear Magnetic Resonance Investigation. *Biophys. Chem.* **2007**, *125*, 320–327. [CrossRef]
27. He, T.; Misuraca, J.C.; Musah, R.A. "Carboranyl-cysteine"-Synthesis, Structure and Self-Assembly Behavior of a Novel α-Amino Acid. *Sci. Rep.* **2017**, *7*, 16995. [CrossRef]

28. Bohren, C.F.; Huffman, D.R. *Absorption and Scattering of Light by Small Particles*, 1st ed.; Wiley-VCH: Weinheim, Germany, 1983; ISBN 0-47-1-29340-7.
29. Carr, B.; Wright, M. *Nanoparticle Tracking Analysis: A Review of Applications and Usage in the Analysis of Exosomes and Microvesicles 2010–2012*; Nanosight: Salisbury, UK, 2013; pp. 1–33.
30. Luo, P.; Roca, A.; Tiede, K.; Privett, K.; Jiang, J.; Pinkstone, J.; Ma, G.; Veinot, J.; Boxall, A. Application of Nanoparticle Tracking Analysis for Characterising the Fate of Engineered Nanoparticles in Sediment-Water Systems. *J. Environ. Sci. (China)* **2018**, *64*, 62–71. [CrossRef]
31. Jarzębski, M.; Bellich, B.; Białopiotrowicz, T.; Śliwa, T.; Kościński, J.; Cesàro, A. Particle Tracking Analysis in Food and Hydrocolloids Investigations. *Food Hydrocoll.* **2017**, *68*, 90–101. [CrossRef]
32. Gercel-Taylor, C.; Atay, S.; Tullis, R.H.; Kesimer, M.; Taylor, D.D. Nanoparticle Analysis of Circulating Cell-derived Vesicles in Ovarian Cancer Patients. *Anal. Biochem.* **2012**, *428*, 44–53. [CrossRef]
33. Gross, J.; Sayle, S.; Karow, A.R.; Bakowsky, U.; Garidel, P. Nanoparticle Tracking Analysis of Particle Size and Concentration Detection in Suspensions of Polymer and Protein Samples: Influence of Experimental and Data Evaluation Parameters. *Eur. J. Pharm. Biopharm.* **2016**, *104*, 30–41. [CrossRef]
34. Filipe, V.; Hawe, A.; Jiskoot, W. Critical Evaluation of Nanoparticle Tracking Analysis (NTA) by NanoSight for the Measurement of Nanoparticles and Protein Aggregates. *Pharm. Res.* **2010**, *27*, 796–810. [CrossRef]
35. Spencer, J.L.; Green, M.; Stone, F.G.A. Metallocarboranes: New Syntheses. *Chem. Commun.* **1972**, 1178–1179. [CrossRef]
36. Kazantsev, A.V.; Akhmetov, S.F.; Tverdokhlebov, A.I. Synthesis and Study of *o*- and *m*-Carborane Derivatives. *Izvestiya Akademii Nauk SSSR Seriya Khimicheskaya* **1973**, *23*, 73–77.
37. Hawthorne, M.F.; Young, D.C.; Garrett, P.M.; Owen, D.A.; Schwerin, S.G.; Tebbe, F.N.; Wegner, P.A. Preparation and Characterization of the (3)-1,2- and (3)-1,7-Dicarbadodecahydroundecaborate(−1) Ions. *J. Am. Chem. Soc.* **1968**, *90*, 862–868. [CrossRef]
38. Harris, R.K.; Becker, E.D.; Cabral de Menezes, S.M.; Goodfellow, R.; Granger, P. NMR Nomenclature: Nuclear Spin Properties and Conventions for Chemical Shifts. IUPAC Recommendations 2001. *Solid State Nucl. Magn. Reson.* **2002**, *22*, 458–483. [CrossRef] [PubMed]
39. CrysAlis-Pro. *Empirical Absorption Correction*; Oxford Diffraction Ltd.: Abingdon, UK, 2014.
40. Sheldrick, G.M. SHELXT-integrated Space-group and Crystal-structure Determination. *Acta Crystallogr. A Found. Adv.* **2015**, *71*, 3–8. [CrossRef]
41. Sheldrick, G.M. Crystal Structure Refinement with SHELXL. *Acta Crystallogr. C Struct. Chem.* **2015**, *71*, 3–8. [CrossRef] [PubMed]
42. Buchanan, R.C.; Park, T. *Materials Crystal Chemistry*; Marcel Dekker: New York, NY, USA, 1997; ISBN 0824797981.
43. Jutzi, P.; Wegener, D.; Hursthouse, M.B. Kristallines $Tl_2B_9H_9C_2Me_2$: Synthese und Festkörperstruktur; ein Beitrag zum Problem "attraktive Tl(I)–Tl(I)-Wechselwirkungen". *Chem. Ber.* **1991**, *124*, 295–299. [CrossRef]